Journal of Environmental Chemical Engineering 11 (2023) 111229

Contents lists available at ScienceDirect

Journal of Environmental Chemical Engineering

journal homepage: www.elsevier.com/locate/jece

Removal of chromium from aqueous solution using a nanocomposite of nickel ferrite and polyaniline doped with 2-naphthalene sulfonic acid

Ruth N. Kasavo, Madhumita Bhaumik, Hendrik G. Brink *

Chemical Engineering Department, University of Pretoria, South Africa

ARTICLE INFO

Editor: <Deepak PANT>

Keywords:
Polyaniline
Nickel ferrite
Chromium
Adsorption
Nanocomposite

ABSTRACT

Chromium is a highly toxic, highly mobile heavy metal commonly found in industrial effluents. This study investigated the efficacy of a nickel ferrite/polyaniline/2-naphthalene sulfonic acid nanocomposite (PANI-NSA/$NiFe_2O_4$) in removing Cr(VI) from solution. NSA doping led to the formation of tubular-shaped rods, enhancing the material's surface area. Key adsorption parameters (pH, adsorbent dosage, agitation time, and initial pollutant concentration) were thoroughly examined and optimized. The adsorption process was notably pH-dependent, with maximal adsorption occurring at pH 2. The findings indicated a remarkable 99.9% removal of Cr(VI) from a 50 mg/L solution with a 25 mg adsorbent dose. Freundlich, Langmuir, and Two-Surface Langmuir isotherm models were tested, with the Two-Surface Langmuir model best describing the experimental results. Kinetics studies revealed rapid adsorption within the initial 30 min, followed by a slower rate, reaching maximum Cr(VI) removal within 24 h. Temperature studies revealed and enhanced adsorption capacity at higher temperatures, with a maximum adsorption capacity of 420.0 mg/g at 45 °C. Thermodynamic analysis indicated an endothermic and spontaneous adsorption process. The mechanism of Cr(VI) removal involved electrostatic attraction, reduction, and surface complexation. PANI-NSA/$NiFe_2O_4$ could be reused for up to five cycles, achieving 99% Cr(VI) removal from a 50 mg/L Cr(VI) solution in the first two cycles. Furthermore, tests on authentic chromium wastewater showed that a 40 mg dose in 50 mL liquid fully removed 50 mg/L Cr(VI). This study underscores the potential of PANI-NSA/$NiFe_2O_4$ for industrial applications in Cr(VI) removal, offering a promising solution for addressing the pressing issue of chromium pollution.

1. Introduction

Pollution of water by heavy metals is one of the most pernicious problems worldwide [1]. As the human population grows, the need for more products and goods increases and this leads to an increase in industries. Effluent streams from these industries containing heavy metals and other pollutants above the allowable discharge limits lead to pollution of water sources and soils. These heavy metal pollutants include chromium, cadmium, copper, arsenic, nickel, mercury, and lead [2]. Due to the inability to biodegrade once released to the environment, the heavy metals may accumulate to even higher concentrations which poses a threat to humans, animals, aquatic life and plants [3].

In aqueous solutions and natural environments, chromium is mostly found in two oxidation states: trivalent (Cr(III)) and hexavalent (Cr(VI)) [4]. Cr(III) occurs naturally in the environment and is not considered a health hazard because it forms a precipitate with soil colloids thus making it stable. On the contrary, Cr(VI) which includes chromate (CrO_4^{2-}) and dichromate compounds ($Cr_2O_7^{2-}$) is an oxidizing agent which has high solubility thus a high presence in wastewater and soils [5,6]. While Cr(III) in water is mainly from natural sources, Cr(VI) is mainly driven by anthropogenic release from chemical and manufacturing industries such as nuclear plants, leather tanning, metal plating, electroplating, paints pigments, paper, and dye production [7,8]. As a result, significantly bio-magnified levels of Cr(VI) enter the terrestrial food chain through fish and then reach people.

Occupational exposure to Cr(VI) has been found to increase the risk of respiratory system cancer with both soluble and poorly soluble chromates being carcinogenic [9–11]. According to Anjum, Mazari [12], Cr(VI) presents several health risks, including mutagenicity, carcinogenicity, neurotoxicity, lung cancer, kidney damage, and skin ulcers. Cr (VI) disguises itself as oxyanions (similar to sulphate, carboxylate, and phosphate) which are needed by the body and diffuses through cell membranes causing damage to cellular proteins, lipid, and other organelles [13,14]. The maximum limit for Cr(VI) in potable water is

* Corresponding author.
E-mail address: deon.brink@up.ac.za (H.G. Brink).

https://doi.org/10.1016/j.jece.2023.111229
Received 16 May 2023; Received in revised form 20 September 2023; Accepted 8 October 2023
Available online 10 October 2023

0.05 mg/L as set by the World Health Organization (WHO) [12,15]. It is therefore important to treat industrial waste before discharging it to water bodies to ensure Cr(VI) concentration does not exceed the maximum allowable limits prescribed by water quality standards.

Several treatment methods have been used in the removal of Cr(VI) from industrial wastewater. These include photocatalysis [16], phytoremediation [17], biological/microbial remediation [18] and electro-chemical reduction [19], and electro-coagulation [20]. These methods often have limitations such as large volume of sludge which makes the process cost and energy intensive. Additionally, these methods suffer from low removal efficiency. Adsorption treatment technology shows advantages over traditional methods due to its simplicity, high efficiency in removing heavy metals and low cost [21,22]. Additionally, when an adsorption method is used, the material can be recovered and recycled through desorption [23]. Different adsorbents have been used for the removal of Cr(VI) from wastewater. These include chitosan based adsorbents [24], carbon materials such as activated carbon [25], carbon nano-tubes [26], metal-organic frameworks [27], Modified rice husk [28], and $FeCl_3$-modified biochar [29].

Electrically conducting polymers such as polyaniline (PANI) and polypyrrole (PPy) have gained interest in the removal of heavy metals owing to the many advantages associated with using them including low cost and ease of synthesis, environmental stability, ease of operation and regeneration, and a high amine group content in their structure which adsorbs and chelates heavy metals via hydrogen bonding or electrostatic interactions [23,30–32]. PANI is ideal for Cr(VI) removal due to its ability to simultaneously act as an electron donor for the reduction of Cr (VI) to less harmful Cr(III) while also providing sites for the adsorption of Cr(VI) [23]. In a study by Lohrentz and co-workers [33], a high adsorption capacity of hexavalent chromium using a polyaniline-Ni(0) nanocomposite was reported. Janmohammadi et al. [34] reported Cr (VI) removal using a waste plastic filter modified with polyaniline and polypyrrole nanoparticles with a maximum Cr(VI) removal capacity of 510.9 mg/g at a pH of 2.0. In another study, a hybrid material of polyaniline/Mg-Al layered double oxides was used for Cr(VI). The maximum adsorption capacity was reported to be 409.77 mg/g at pH 2.0 [35]. Even though polymers have shown such a remarkable potential for the removal of heavy metals, when used on their own, these conducting polymers tend to have low adsorption capacity due to decreased surface area caused by agglomeration of particles. Additionally, it is a challenge to separate the polymer adsorbent from large volumes of solutions after adsorption [36]. This makes it hard to recover and recycle the adsorbent. Magnetic nanoparticles are being used to produce composites of polymers because magnetic separation via the application of an external magnetic field can be used to overcome the challenge of separation and the process is easier than filtration and centrifugation.

According to Gupta, Jain [37], ferrites of general formula $A-Fe_2O_4$ e.g. $NiFe_2O_4$, $CoFe_2O_4$, $MnFe_2O_4$ and $CuFe_2O_4$ have been applied in many areas such as in microwave devices, gas sensor, colour imaging, electronic devices, ferrofluids magnetic drug delivery, among others. This is due to their high specific heat capacity, high electrical selectivity, low melting point, and high corrosion resistance[37,38]. Among the available magnetic sorbents, inorganic spinel ferrites and their composite materials have been widely used in water treatment due to their unique advantages of magnetic and chemical stability. However, the spinel nickel ferrite ($NiFe_2O_4$) is the most significant due to the ferromagnetic properties which originate from the parallel alignment of the spins of the Fe^{3+} ions on the tetrahedral sites and both the $Ni^{2+}$and Fe^{3+}ions on the octahedral sites [39].

Even though Agrawal and Singh [40] used $NiFe_2O_4$-PANI nanocomposite in a previous study, they reported a very low maximum adsorption capacity (12.19 mg/g). In this study, we investigated the effectiveness of 2-naphthalene sulfonic acid (2-NSA) doped polyaniline and nickel ferrite particle nanocomposite (PANI-NSA/$NiFe_2O_4$) produced via an in-situ chemical oxidative polymerization method in removing of Cr(VI) from aqueous solution. Batch experiments were conducted to evaluate optimal conditions for the adsorption of Cr(VI) by PANI-NSA/$NiFe_2O_4$.

2. Materials and methods

2.1. Chemical reagents and standards

Aniline (C_6H_7N), ammonium persulfate ($APS(NH_4)_2S_2O_8$,), 2-Naphthalene sulfonic acid (2-NSA, $C_{10}H_8O_3S$), potassium dichromate ($K_2Cr_2O_7$), 1,5-diphenylcarbazide (DPC) and nickel ferrite ($NiFe_2O_4$) nano powder (<50 nm particle size) were purchased from Sigma Aldrich. Sulphuric acid (H_2PO_4, 98 wt%), nitric acid (HNO_3, 98 wt%), sodium hydroxide (NaOH) and methanol (CH_3OH) were obtained from Fisher Scientific and Glassworld. All the chemicals were used as received without any further treatment.

2.2. Preparation of chromium stock solution

The Cr(VI) stock solution (1000 mg/L) of Cr(VI) was prepared by dissolving 1.414 g of potassium dichromate ($K_2Cr_2O_7$) in ultrapure water in a 1000 mL volumetric flask. Fresh working solutions for each experiment were prepared from the stock solution.

2.3. Preparation of 1,5-DPC solution for Cr(VI) analysis

1,5-DPC solution was prepared by dissolving 125 mg of 1,5-DPC in 25 mL of methanol. 7 mL of H_2SO_4 (98%) was mixed with 125 mL deionized water and added to the above solution to make a 250 mL total volume.

2.4. Synthesis of PANI and PANI/$NiFe_2O_4$ PNCs

PANI-NSA/$NiFe_2O_4$ PNC was fabricated by emblematic in-situ oxidative polymerization method which was adapted from elsewhere [41]. In this synthesis method, 0.2 mL aniline and a predetermined amount of $NiFe_2O_4$ nano-powder were mixed with 80 mL of 2-NSA solution (0.416 g of 2-NSA dissolved in 80 mL of deionized water) under ultrasonic agitation for 15 min. During the agitation period, aniline reacted with 2-NSA to form NSA-ANI micelles containing $NiFe_2O_4$ nano-powder. Thereafter, 0.456 g of APS dissolved in 5 mL of deionized water in a separate beaker was added to the above $NiFe_2O_4$ suspension and sonicated for another 1 min. The mixture was labelled (PANI-NSA/$NiFe_2O_4$, wt%) and kept undisturbed under room temperature for 24 h for in-situ polymerization. After 24 h the product was vacuum filtered and washed with deionized water. Further washing with methanol was done to remove any possible oligomers. The final PNC product was dried in a vacuum oven at 60 °C for 24 h. Pure PANI was synthesized in the same manner without adding nickel ferrite.

2.5. Chromium analysis methods

A UV VIS spectrophotometer at 540 nm wavelength was used to determine the final concentration of Cr(VI) ions in the aqueous medium after adsorption. The instrument's calibration curve used standard solutions of 1 mg/L, 0.5 mg/L, 0.25 mg/L, and 0.1 mg/L of Cr(VI). Flame Atomic Absorption Spectrometer (FAAS) was used to determine the total chromium after adsorption. Standard solutions of 1 mg/L, 2.5 mg/L and 5 mg/L were used for the FAAS calibration.

2.6. Preliminary studies

It was noted from literature [42,43] that acidic pH values and especially pH 2 gave a better removal percentage of Cr(VI) from solution hence initial pH of 2 was chosen for the preliminary studies.

Preliminary studies were done to determine the optimum loading of

$NiFe_2O_4$ in the PNC as well as the initial dosage for the batch experiments. To determine the optimum loading, the following masses of $NiFe_2O_4$ were used in the PNC (10, 20, 25, 50, 1and 00 mg). The obtained PNCs were used to remove 100 mg/L of Cr(VI) from a 25 mL solution at pH 2. The solutions were shaken in the thermostatic water bath shaker at 25 °C with a shaking speed of 200 rpm. The initial pH of the solution was adjusted using HNO_3 (0.1 M) and/or NaOH (0.1 M).

It was observed that the loading of 10 mg of $NiFe_2O_4$ on the PNC led to a 94.9% removal of Cr(VI) from the solution. Changing the loading of $NiFe_2O_4$ from 10 to 20 mg led to a very slight increase in the percentage removal of Cr(VI) (95.7%) while any further increase from 20 mg led to a decline in the percentage removal to 80.8% at 100 mg loading. Even though a higher loading of $NiFe_2O_4$ would increase the effectiveness of the material regarding magnetic properties, the loading mass of 10 mg was used in the batch studies.

Initial studies to determine the optimum dose for batch experiments were done where the dose of PNC was varied from 5 mg to 40 mg while the solution pH, the initial Cr(VI) concentration and the sample volume were kept constant at 2, 25 mg/L and 25 mL respectively. It was observed that complete removal of Cr(VI) was observed for all the dosages and therefore for the batch experiment, the initial Cr(VI) concentration and sample volume were both increased to 50 mg/L and 50 mL respectively.

2.7. Batch adsorption studies

Effect of initial Cr(VI) concentration, effect of temperature, effect of dosage and initial Cr(VI) pH effect experiments were conducted in a thermostatic water bath shaker agitated at 200 rpm for 24 h using 100 mL glass bottles containing 50 mL solutions of Cr(VI). Effect of agitation time experiments were conducted using an overhead stirrer on a 1000 mL beaker filled with 500 mL solutions of Cr(VI) mixed at a speed of approximately 200 rpm. All experiments were carried out twice and the average value was reported.

2.7.1. Effect of dosage

To test the effect of PANI-NSA/$NiFe_2O_4$ dosage, Cr(VI) solutions were contacted with PANI-NSA/$NiFe_2O_4$ nanocomposite whose dose was varied between 5 and 40 mg. The different masses of the adsorbent were weighed using a 4-decimal point digital mass balance. The efficiency (% removal) of Cr(VI) was calculated using Eq. (1):

$$\%\ \text{removal} = \frac{C_o - C_e}{C_o} \times 100 \tag{1}$$

where $C_o$and C_e are the initial and equilibrium concentration of Cr (VI), respectively, in mg/L.

2.7.2. Effect of solution pH

To analyse the effect of the initial Cr(VI) solution pH on the removal of Cr(VI) by the synthesized PANI-NSA/$NiFe_2O_4$, the initial pH of the Cr (VI) solutions was adjusted to pH values between 2 and 11 before contacting with 25 mg of PANI-NSA/$NiFe_2O_4$ nanocomposite.

2.7.3. Point of zero charge

The point of zero charge (PZC) study was done following a method described elsewhere [44]. 0.125 g of adsorbent was added in 25 mL deionized water into several sample bottles, later the pH was adjusted between 2 and 12 units with solutions of HCl 1.0 M and NaOH 1.0 M. The final pH was measured after 24 h.

2.7.4. Effect of initial concentration

To test the effects of initial concentration, Cr(VI) solutions with concentrations varied between 50 and 400 mg/L were prepared from the stock solution and contacted with 25 mg of PANI-NSA/$NiFe_2O_4$ nanocomposite at pH 2. The equilibrium capacity was determined using Eq.(2):

$$Q_e = \frac{C_o - C_e}{m} \times V \tag{2}$$

Where Q_e (mg/g) is the amount of Cr(VI) adsorbed per unit mass of adsorbent at equilibrium, m is the mass of the adsorbent (g) and V is the sample volume (L). To test the effect of temperature the effects of initial concentration experiment was carried out at 3 different temperatures (25 °C, 35 °C and 45 °C) in a thermostatic shaker. The results were used for isotherm modelling. Table 1 summarizes the conditions for isotherm experiments.

2.7.5. Effect of contact time

The effect of contact time was studied by contacting 500 mL Cr(VI) of solution with 250 mg of PANI-NSA/$NiFe_2O_4$ nanocomposite in a beaker continuously stirred at 200 rpm with a non-magnetic stirrer. Three initial Cr(VI) concentrations (50, 100 and 200 mg/L) were studied over a 6 h period. Sample volumes of 4 mL were drawn from the beaker in selected time intervals between 0 and 360 min and analysed for residue Cr(VI) and Cr(III) concentration. The adsorption capacity of the adsorbent, Q_t (mg/g) at any time was obtained from Eq.(3):

$$Q_t = \frac{C_o - C_t}{m} \times V \tag{3}$$

Where C_t (mg/L) is Cr(VI) concentration in the solution at any time t. The results obtained from this experiment were used for kinetic model fitting.

2.7.6. Effect of other ions

To test the effect of co-existing ions on the adsorption of Cr(VI), copper (Cu^{2+}), zinc (Zn^{2+}), sulfate (SO_4^{2-}), and nitrate (NO_3^-) ions were used in a mixed (binary) sorption system described by [45]. In this experiment, a 50 mL aqueous solution containing an initial concentration of 50 mg/L of Cr(VI) and initial concentrations of the co-existing ions (50, 100, 150 mg/L) was mixed with 25 mg of PANI-NSA/$NiFe_2O_4$ and shaken at room temperature for 24 h after which it was analysed for Cr(VI) concentration.

2.7.7. Desorption studies and re-usability

To test the regeneration of PANI-NSA/$NiFe_2O_4$, 25 mg of PANI-NSA/$NiFe_2O_4$ was conducted with 50 mL of 50 mg/L Cr(VI) solution in a 100 mL glass bottle. After 24 h, a centrifuge was used to separate the solid material residual from the supernatant. The supernatant was analysed for Cr(VI).

The residual was washed with de-ionized water to remove excess Cr (VI) before mixing with 50 mL of 1 M NaOH and sonicating for 5 min. The Cr(III) concentration was calculated from the difference between the total chromium and Cr(VI) concentration. The same desorption step was repeated with HNO_3 to remove Cr(VI) ions. The residue recovered from the two desorption steps was mixed with de-ionized water and centrifuged for 25 mins at 9000 rpm before separating. It was then contacted with a new Cr(VI) solution for a new adsorption cycle.

2.7.8. Test on authentic chromium water

This study utilized industrial wastewater containing chromium obtained from a chrome plating facility located in the Tshwane Region of South Africa. To enable a fair comparison with experimental work involving synthetic chromium wastewater, the initial concentration of Cr(VI) in the wastewater was measured and then diluted to a concentration of 50 mg/L using de-ionized water. Subsequently, 50 mL of this diluted solution was mixed with varying doses of PANI-NSA/$NiFe_2O_4$ (15, 25, 30, and 40 mg) after adjusting the pH to 2. After a 24-hour period of shaking, the final concentration of Cr(VI) was determined.

Table 1
Summary of studied parameters for adsorption isotherms.

Experiment	Temperature (°C)	Adsorbent dosage (mg)	Initial Cr (VI) concentration (mg/L)	Initial pH of Cr (VI) solution	Experimental time (hours)
1	25	25	50, 100, 150, 200, 250, 300, 350, 400	2 ± 0.03	24
2	35	25	50, 100, 150, 200, 250, 300, 350, 400	2 ± 0.03	24
3	45	25	50, 100, 150, 200, 250, 300, 350, 400	2 ± 0.03	24

2.8. Characterization

A Micrometrics TriStar II BET analyser (Micrometrics Inc., Norcross, GA) was used to obtain the 124 Brunauer-Emmett-Teller (BET) specific surface area and pore size of PANI-NSA and PANI-NSA/$NiFe_2O_4$ nanocomposite. Liquid nitrogen at 77 K was used for the measurements. To remove impurities and moisture from the samples before analysis, degassing was done by vacuum drying for 10 h at a temperature of 100 °C. A field emission scanning electron microscope (Zeiss Ultra PLUS FEG SEM) and a high-resolution transmission electron microscope (Jeol 2100 F FEG TEM) were used to obtain morphological images of PANI-NSA and PANI-NSA/$NiFe_2O_4$ and Energy Dispersive X-Ray (EDX) composition analysis of PANI-NSA/$NiFe_2O_4$. The morphology of the material was checked on the material as synthesized without coating. X-ray photoelectron spectroscopy (XPS) was used to characterize the PANI-NSA/$NiFe_2O_4$ before and after Cr(VI) adsorption with a Thermo ESCAlab 250 Xi (USA). The samples were washed with water and methanol and dried at 60 °C after adsorption. Silica gel was placed in the container with the samples to remove moisture. Functional groups of the PANI-NSA/$NiFe_2O_4$ nanocomposite was obtained from IR spectra using a Perkin-Elmer (USA) Fourier transform infrared spectrometer (Spectrum 750 S spectrometer). To explore the temperature-dependent magnetic properties of the composite and its components, a Physical Property Measurement System (PPMS) from Quantum Design (USA) with a Vibrating Sample Magnetometer (VSM) measurement mode was used. X-ray diffraction (XRD) crystalline profiles for $NiFe_2O_4$ and PANI-NSA/$NiFe_2O_4$ were recorded on a PANanalytical X′pert PRO diffractometer.

3. Results and discussions

3.1. Characterization

BET results indicated that the surface area of PANI-NSA/$NiFe_2O_4$ (26.513 $\frac{m^2}{g}$) is higher than that of PANI-NSA (21.773 $\frac{m^2}{g}$) which shows that synthesizing a composite of PANI and $NiFe_2O_4$ significantly increases the surface area of the material. SEM images of synthesized pure PANI-NSA and PANI-NSA/$NiFe_2O_4$ are shown in Fig. 1(a) and Fig. 1(b). From the images, it can be observed that PANI-NSA forms rod-like structures whose surface is smooth while PANI-NSA/$NiFe_2O_4$ composite forms rods with a rough surface. The rough surface is linked to

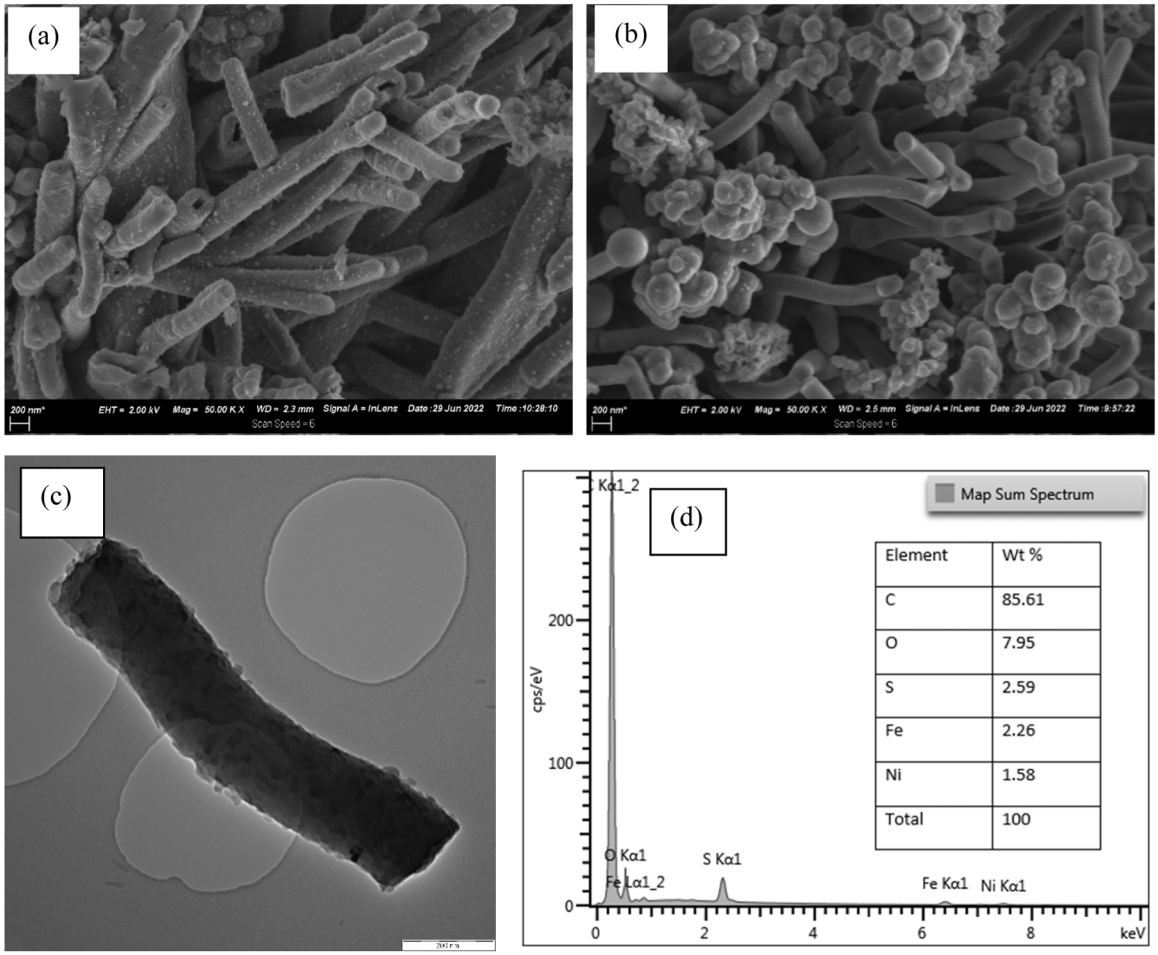

Fig. 1. SEM images of (a) PANI-NSA/$NiFe_2O_4$, (b) PANI-NSA (b) and (c) TEM image of PANI-NSA/$NiFe_2O_4$ and (d) EDX analysis of PANI-NSA/$NiFe_2O_4$.

$NiFe_2O_4$ attaching on the forming PANI-NSA. This increases the pore diameter and provides more surface for Cr(VI) adsorption. It is also observed that PANI-NSA exhibits noticeable agglomeration while PANI-NSA/$NiFe_2O_4$ has less agglomeration with most rods occurring individually. Fig. 1(c) shows the TEM analysis of PANI-NSA/$NiFe_2O_4$. It can be noted that the $NiFe_2O_4$ nanoparticles are completely encapsulated in the PANI-NSA/$NiFe_2O_4$ structure (signified by the presence of dark spots). This confirms that this method allows for the encapsulation of $NiFe_2O_4$ in the forming rods of aniline during the polymerization. A study by Bhaumik et al. [46] yielded similar results. The EDX analysis shown in Fig. 1(d) confirms the presence of Ni and Fe ions in the structure of the PANI-NSA/$NiFe_2O_4$. The EDX results also show that the polymer (PANI-NSA) is the main component of the PANI-NSA/$NiFe_2O_4$ due to the higher composition of C and H.

The species of PANI-NSA/$NiFe_2O_4$ as well as the valence of chromium on the surface of PANI-NSA/$NiFe_2O_4$ were determined by XPS. The results obtained from XPS before and after treatment with Cr(VI) solution are shown in Fig. 2(a). C1s, N1s, O1s, and S2p are observed at the corresponding binding energies of 284.9, 399.3, 531.8, 168.2 eV suggesting the presence of mainly PANI in the PANI-NSA/$NiFe_2O_4$ nanocomposite. Additionally, a Cr2p peak was observed at 577.3 eV in the after-treatment XPS spectrum as shown in Fig. 2(b) confirming the adsorption of Cr(VI) on the surface of the PANI-NSA/$NiFe_2O_4$ nanocomposite. No peaks suggested the presence of $NiFe_2O_4$ on the surface of the nanocomposite. This could be due to the low composition of $NiFe_2O_4$ in the nanocomposite. Another possible explanation is that since XPS is a surface method of analysis, it may not detect the Ni and Fe ions since $NiFe_2O_4$ nanoparticles are well encapsulated in the PANI-NSA structure. The presence of S2p peaks in the nanocomposite indicates the presence of a sulfur group due to the doping of PANI with NSA. The deconvoluted S2p peaks in Fig. 2(b) show that the SO_3^{2-} group which was present before treatment with Cr(VI) solution (Fig. 2(a)) disappears after treatment with Cr(VI) solution indicating that SO_3^{2-} group takes part in the removal of chromium. The N1s spectrum in the PANI-NSA/$NiFe_2O_4$ before treatment with Cr(VI) solution was deconvoluted into 2 distinct curves with peaks at 399.2 and 400.7 (Fig. 2(c,d)) while two curves with peaks at 399.3 and 401.2 are observed in the PANI-NSA/$NiFe_2O_4$ after treatment with Cr(VI) solution (Fig. 2(e,f)). The peaks at 399.2 and 399.3 are related to the undoped amine groups ($-NH-$) while the peaks at 400.7 and 401.2 are related to the doped amine ($-NH^+$) and ($-NH_4^+$) cations associated with the ammonium persulfate used in oxidation of aniline in the polymerization process.

The FTIR spectra of PANI-NSA/$NiFe_2O_4$ nanocomposite, $NiFe_2O_4$

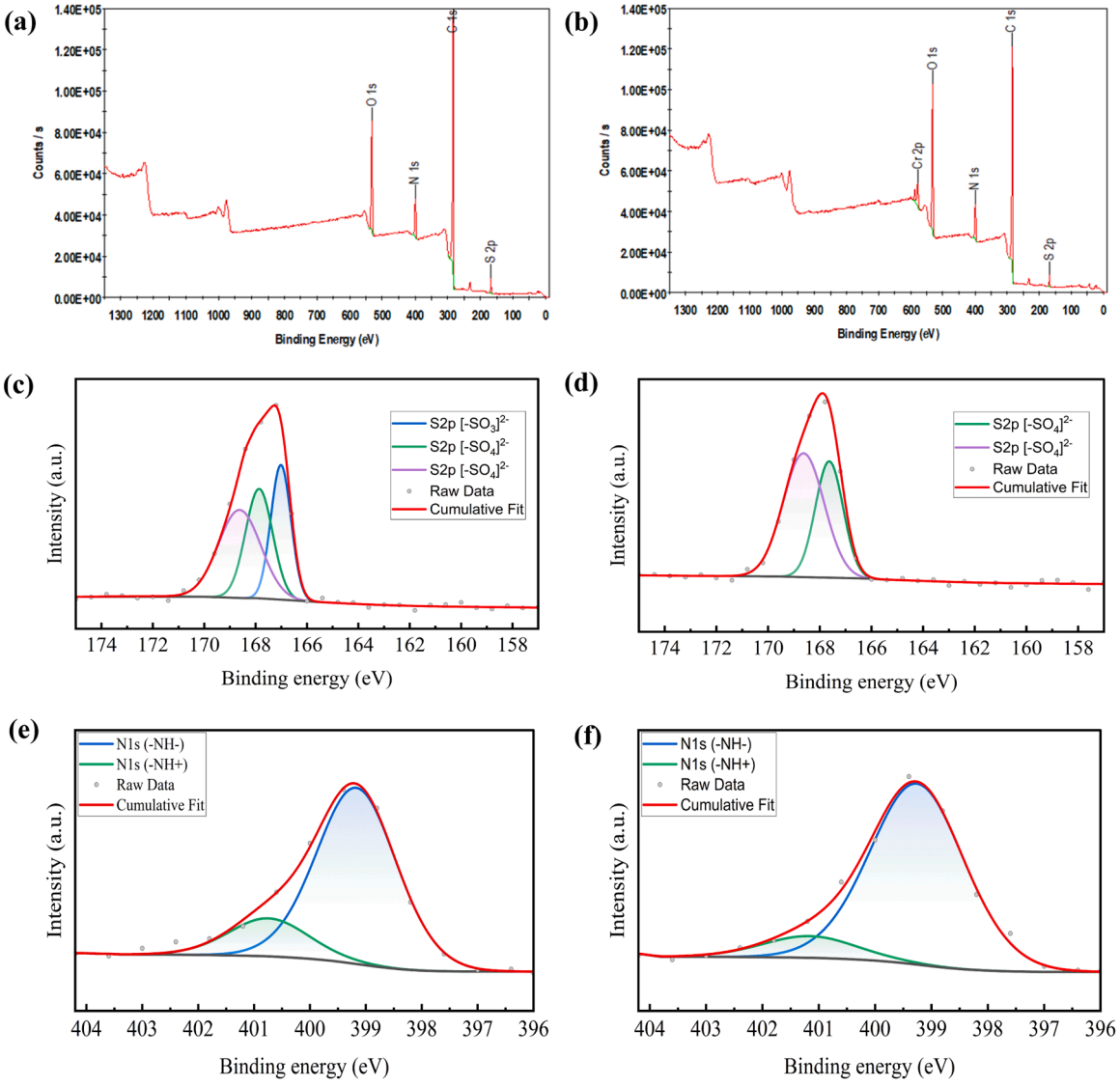

Fig. 2. XPS survey of PANI-NSA/$NiFe_2O_4$ (a) before and (b) after treatment with Cr(VI) and deconvoluted peaks of before and after treatment with Cr(VI) for: (c, d) S2p, (e, f) N1s.

nanoparticles and PANI are shown in Fig. 3. Peaks of PANI-NSA are observed at 1575, 1488, 1299, 1238, 1048, 1028, 829, and 670 cm^{-1}. The peaks at 1575 and 1488 are associated with functional groups of C –C bond of quinonoid and benzenoid rings, peak at 1299 is associated with C-N stretching of the B rings as a result of protonation of PANI [47]. The peak at 1238 represents –C(CO)O- stretching [48], at 1048 the presence of C-O stretching [49], and the peak at 829 is associated with C-H bonds in aromatic rings, peaks at 1028 and 670 are associated with doped -SO_3H group [50].

Fig. 4 depicts the magnetic hysteresis loops of PANI-NSA, $NiFe_2O_4$, and PANI-NSA/$NiFe_2O_4$ composite. According to the graph, the magnetization of PANI-NSA/$NiFe_2O_4$ and $NiFe_2O_4$ increased and tended to reach saturation as the magnetic field increased. The magnetization values are 25 and 2.5 emu/g for $NiFe_2O_4$ and PANI-NSA/$NiFe_2O_4$ respectively. As a result, the magnetization curves show that the PANI-NSA/$NiFe_2O_4$ composite has good magnetic properties.

Fig. 5 gives the XRD pattern of $NiFe_2O_4$ and PANI-NSA/$NiFe_2O_4$ nanocomposite. The diffraction peaks observed at 2θ of 21.7° (111), 35.8° (220), 41.8° (311), 43.3° (222), 51.3° (400), 63.5° (422), 67.5° (511) and 75.0° (440) are the characteristic peaks of $NiFe_2O_4$ (PDF Card 96–591–0065). The characteristic peaks are also observed on the PANI-NSA/$NiFe_2O_4$ nanocomposite XRD pattern even though they broaden out. This confirms the interaction between PANI-NSA and $NiFe_2O_4$ in the formation of PANI-NSA/$NiFe_2O_4$ nanocomposite. Additionally, these broader peaks could be due to $NiFe_2O_4$ nanoparticles being covered by PANI-NSA.

3.2. Effect of solution pH

Solution pH affects the Cr(VI) removal efficiency because it determines the charge on the surface of the adsorbent as well as the degree of ionization and speciation of the adsorbate which affects the ions available in the aqueous solutions.[40]. Fig. 6(a) shows the effect of initial solution pH on the removal efficiency of Cr(VI) by PANI-NSA/$NiFe_2O_4$. It is observed that the percentage removal of Cr(VI) by PANI-NSA/$NiFe_2O_4$ decreases with an increase in the pH of the solution with the maximum removal observed at pH 1 and 2. The pH dependence of Cr(VI) removal rate by PANI-NSA/$NiFe_2O_4$ is due to the existence of different chromium species at different pH values and change in the charge of the PANI-NSA/$NiFe_2O_4$ surface which affects the adsorption efficiency. In acidic solution conditions (pH values between 1 and 6), $HCrO_4^-$ predominantly coexists with $Cr_2O_7^{2-}$ while at higher pH values (pH values above 6), $Cr_2O_7^{2-}$ is the predominant species.

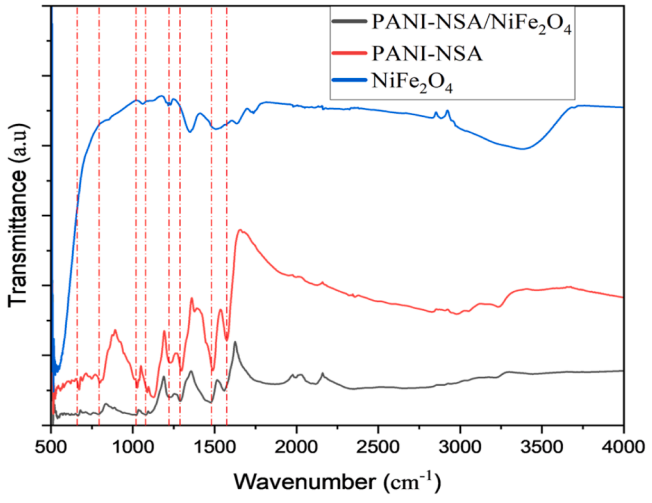

Fig. 3. FTIR spectrum of PANI-NSA, Ni Fe_2O_4 and PANI-NSA/$NiFe_2O_4$ composite. The red dashed lines represent the characteristic peaks associated with PANI-NSA.

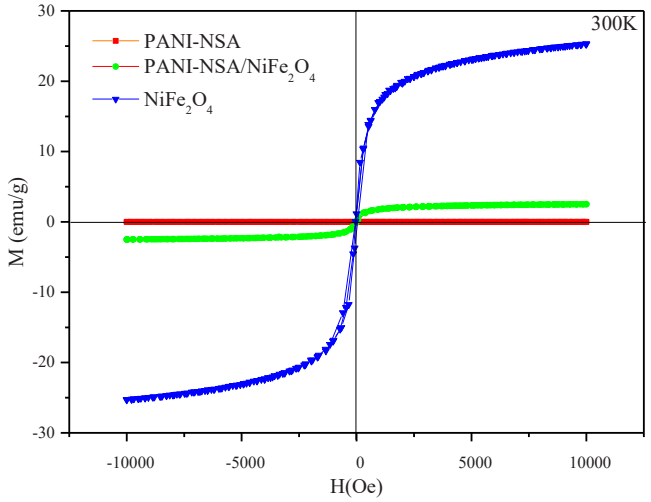

Fig. 4. Magnetic hysteresis loops of PANI-NSA, Ni Fe_2O_4, and PANI-NSA/$NiFe_2O_4$ composite.

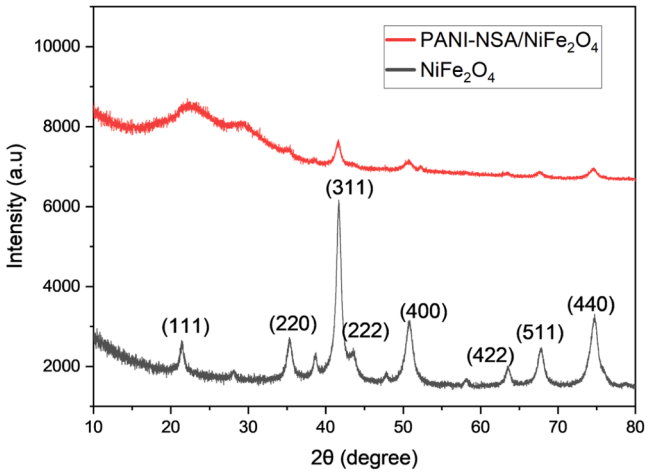

Fig. 5. XRD pattern of PANI-NSA/Ni Fe_2O_4 and Ni Fe_2O_4.

Additionally, in acidic conditions, the surface of PANI-NSA/$NiFe_2O_4$ is highly protonated due to the presence of NH^+ functional groups. This leads to a high electrostatic attraction between the oxyanions of Cr(VI) and the positively charged surface of the adsorbent. As the pH increases, the positive charge on PANI-NSA/$NiFe_2O_4$ surface decreases and thus a decline in the removal rate due to the repelling nature between the surface and the oxyanions. Additionally, at pH above 6 there is a high abundance of hydroxyl ions which compete with the oxyanions of Cr(VI) for the active sites thus leading to a further decrease in Cr(VI) removal. [40] and [51] reported a similar trend in the effect of pH on the Cr(VI) removal efficiency.

3.3. Determination of the point of zero charge

The pH of the solution is important in cation adsorption because it affects the speciation and ionisation of adsorbent active sites [52]. The net charge of the adsorbent affects the protonation-deprotonation behaviour of the adsorbent which is relevant in explaining the mechanism of adsorption. The point of zero charge determines the charge on the surface of the adsorbent and hence the electrostatic interactions between the adsorbent and the adsorbate. At a solution pH equal to the point of zero charge pH (pHpzc), the adsorbent's surface charge is neutral. When the pH of the solution is less than pHpzc, the adsorbent

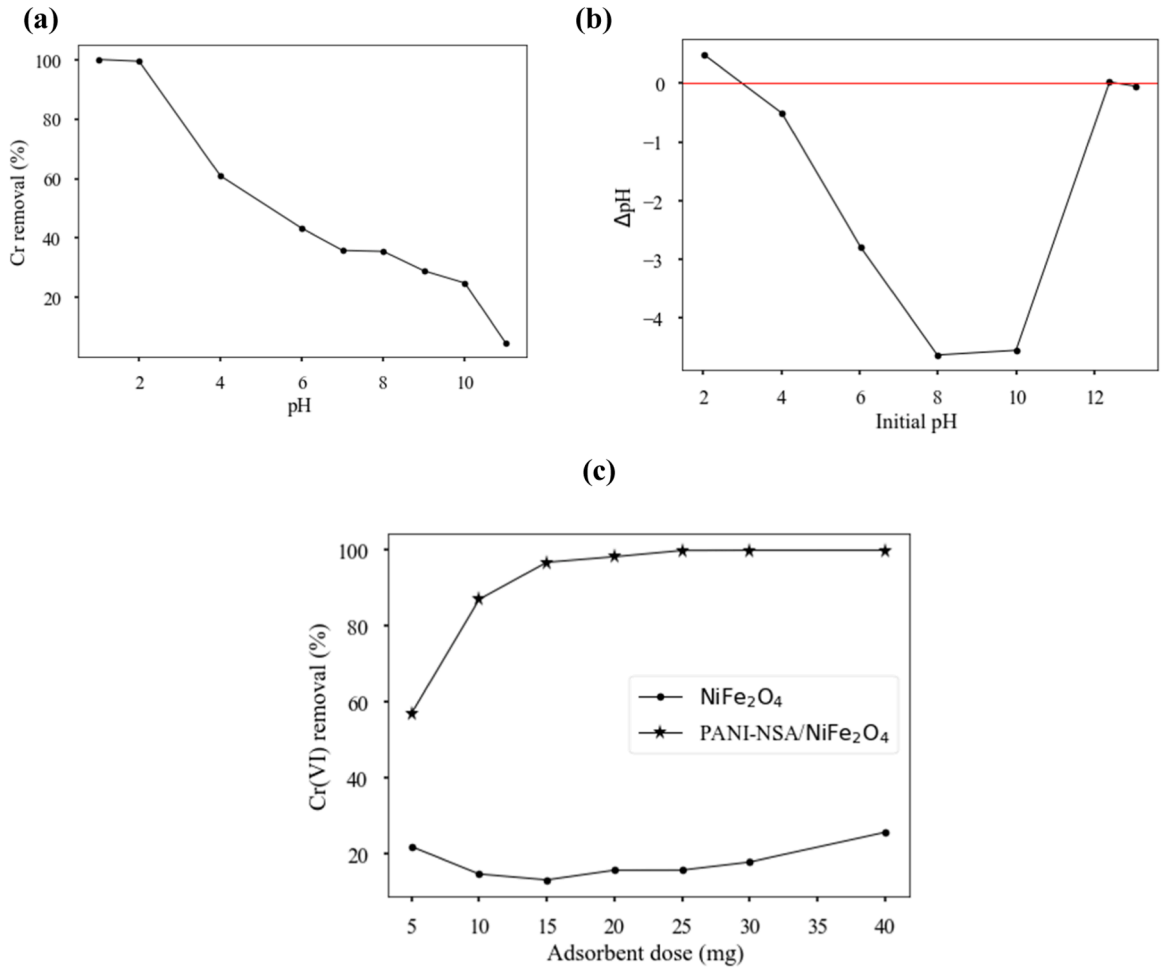

Fig. 6. Effect of (a) pH, (b) point of zero charge of PANI-NSA/$NiFe_2O_4$ and (c) dosage on Cr(VI) removal efficiency.

operates as a positively charged surface; whereas when it is greater than pHpzc, the adsorbent behaves as a negatively charged surface [53]. From Fig. 6(b), it is observed that the pHpzc of PANI-NSA/$NiFe_2O_4$ is 2.8 ± 0.1 (the point where the initial pH = final pH). This shows that PANI-NSA/$NiFe_2O_4$ surface is positively charged at pH below 2.8 which attracts the negatively charged $HCrO_4^-/Cr_2O_7^{2-}$ species, hence the higher Cr(VI) removal efficiency observed at lower pH values. At pH above 2.8, the surface of PANI-NSA/$NiFe_2O_4$ is negatively charged which repels the CrO_7^{2-} ions hence lower Cr(VI) removal efficiency. These results are consistent with the effect of pH results which show a rapid drop in the Cr (VI) removal efficiency when the pH is increased from 2 to 4.

Fig. 6(c) shows the effect of the dose on the removal of Cr(VI) from the aqueous solution. It can be observed that the removal efficiency from a 50 mL of 50 mg/L Cr(VI) solution increases from 56.9% for 5 mg adsorbent mass to 99.9% for 25 mg adsorbent mass. This is due to an increase in surface area which translates to more active sites being available for adsorption. The removal percentage does not change with any further increase in adsorbent dose due to the adsorbate (Cr(VI)) becoming limiting. This also shows that an adsorbent loading of 0.5 g/L is enough to remove Cr(VI) from 50 mL solution with an initial Cr(VI) concentration of 50 mg/L. These results were consistent with two other previous studies [4], [45] and confirm that PAN-I-NSA/$NiFe_2O_4$ nanocomposite has a high affinity for Cr(VI) removal. In another study using a nickel ferrite-polyaniline material synthesized through oxidative polymerization, [40] found that an adsorbent dosage of 0.5 g/10 mL attained a 70% removal of Cr(VI) from 10 mL of 10 mg/L initial Cr(VI) concentration which confirms that the PANI-NSA/$NiFe_2O_4$ synthesized in this study has a higher removal capacity. Comparing the performance of pure $NiFe_2O_4$ to that of the PAN-I-NSA/$NiFe_2O_4$ nanocomposite shows that pure PAN-I-NSA/$NiFe_2O_4$ nanocomposite performs better than pure $NiFe_2O_4$ implying that modifying the nanoparticles with PANI-NSA increases the surface area for adsorption.

3.4. Adsorption isotherms

Fig. 7(a) shows the effect of initial Cr(VI) concentration. It is observed that the percentage removal of Cr(VI) declines with an increase in initial Cr(VI) concentration. This is due to enough active sites not being available for the adsorption. Since the number of active sites is not increasing, increasing the concentration of Cr(VI) does not lead to any significant increase in the Cr(VI) uptake. It also observed that the percentage removal increases with an increase in temperature signifying that the process is endothermic. The maximum removal of Cr(VI) is observed at 45 °C for all concentrations hence this is the optimum temperature recommended for this process.

Fig. 7(b, c, d) shows the fitting of non-linearized Langmuir, Freundlich and Two-surface Langmuir isotherm models on the experimental data at different temperatures. The increasing value of Q_e with an increase in temperature for all models confirms that the adsorption of Cr(VI) on PANI-NSA/$NiFe_2O_4$ is an endothermic process. The various adsorption parameters calculated from these model fittings are given in Table 2. The coefficient of determination (R^2) is observed to decrease in the order: Two surface Langmuir, Freundlich and Langmuir indicating that the Two-surface Langmuir isotherm model best fits the isotherm data confirming that adsorption of Cr(VI) occurs on more than one

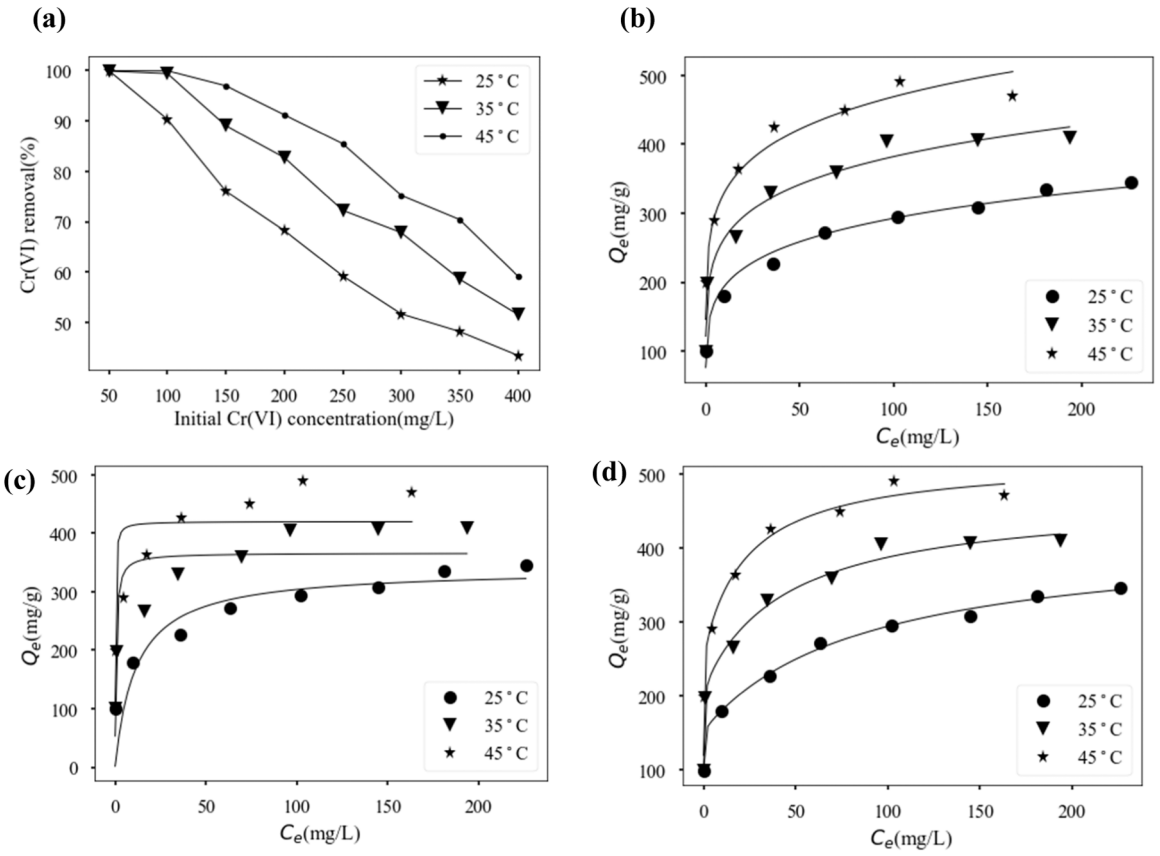

Fig. 7. (a) Effect of initial concentration and (b) Freundlich, (c) Langmuir and (d)Two-surface Langmuir isotherm fitting.

Table 2
Parameters from the isotherm models calculations.

Isotherm model	Differential form	Fitted parameters	Temperature		
			25 °C	35 °C	45 °C
Langmuir	$Q_e = \frac{K_L Q_{max} C_e}{1 + K_L C_e}$	Q_{max} $(mg.g^{-1})$	338.93	366.02	420.0
		K_L (L/mg)	0.0864	1.9776	6.5238
		R^2	0.754	0.8681	0.8176
Freundlich	$Q_e = K_F(T)C_e^{1/n_F}$	K_F $\left(L^{\frac{1}{n_F}} mg^{1-\frac{1}{n_F}} g^{-1}\right)$	128.81	181.5	232.2
		n_F	5.61	6.19	6.56
		R^2	0.9769	0.9798	0.9616
Two-surface Langmuir	$Q_e = \frac{k_{L,1}(T)Q_{max,1}C_e}{1 + k_{L,1}(T)C_e} + \frac{k_{L,2}(T)Q_{max,2}C_e}{1 + k_{L,2}(T)C_e}$	$K_{L,1}(L/mg)$	0.01145	0.02194	0.0416
		$K_{L,2}(L/mg)$	∞	∞	∞
		$Q_1(mg.g^{-1})$	262.55	254.41	260.14
		$Q_2(mg.g^{-1})$	153.89	212.52	259.32
		R^2	0.9966	0.9912	0.9868

surface sites. The observation that $K_{L2} \rightarrow \infty$ indicates that the second surface corresponds to irreversible adsorption, i.e., initially surface corresponding to K_{L2} and Q_{max2} (second surface) is saturated irreversibly, after which the surface corresponding to K_{L1} and Q_{max1} (first surface) reversibly adsorbs the adsorbate. This results in $C_e = 0$ values for low initial concentrations of adsorbate, at higher initial concentrations the second surface saturates, and the first surface starts to reversibly adsorb the adsorbate. It is noteworthy that the first surface has a $Q_{max,1}$ which was nearly independent of temperature, while the second surface exhibited a significant increase in $Q_{max,2}$ for increased temperature.

The Freundlich isotherm second best describes the isotherm data in this study. The fitted parameter $n_F > 1$ for all temperatures implies that adsorption is favourable at all the studied temperatures. For Langmuir isotherm model, the K_L values increased with an increase in temperature indicating an increased affinity for Cr(VI) by PANI-NSA/$NiFe_2O_4$ with an increase in temperature. The calculated Q_{max} values are comparatively higher when compared to those of other studies [40,42,51,54] which further confirms that the synthesized PANI-NSA/$NiFe_2O_4$ has a very high affinity for Cr(VI) and therefore suitable for industrial applications.

3.5. Thermodynamic Properties

Thermodynamic properties of adsorption such as standard enthalpy change (ΔH°), standard entropy change (ΔS°), and standard Gibbs free energy change (ΔG°) were calculated from Eq.(4).

$$\begin{cases} \Delta G^\circ = -RT\ln(K) = \Delta H^\circ - T\Delta S^\circ \\ \therefore \ln(K) = -\frac{\Delta H^\circ}{RT} + \frac{\Delta S^\circ}{R} \end{cases} \quad (4)$$

Where K is the thermodynamic equilibrium constant, R is the gas constant (J/mol/K), and T is the temperature in K. The values of ΔS°, ΔH° and ΔG° were calculated from the intercept and the slope of the linear plot of $\ln K$ vs 1/T where the isotherm constants (K_F and K_{L1}) were used to calculate K using Eqs. 5 and 6 [55]. Due to the poor fit of the data to the Langmuir Isotherm (see Table 3), the results for the Langmuir isotherm were not used for the thermodynamic analysis.

$$K = K_L \times M_w \times 55.5 \times 10^3 \quad (5)$$

$$K = K_F \times \rho \times \left(\frac{10^6}{\rho}\right)^{1-\frac{1}{n_F}} \quad (6)$$

With M_W the molecular weight of the adsorbate (116 g/mol), 55.5 mol/L the molar concentration of pure water (mol/L), and ρ the density of pure water (1 g/mL). The various thermodynamic parameters calculated from these models are given in Table 3.

The results for the Freundlich and Two-surface Langmuir Isotherm models were significantly similar with positive values of $\Delta S^{\circ} = 246.8$ and 263.7 J/mol/K calculated, respectively. This indicates an increase in randomness at the interface of the solution and the catalyst (PANI-NSA/$NiFe_2O_4$). Additionally, the calculated values of $\Delta H^{\circ} = 30.3$ and 50.8 kJ/mol, for the Freundlich and Two-surface Langmuir Isotherm models respectively, indicated physical and reversible adsorption processes [56]. The positive values of ΔH° also confirm endothermic adsorption process. Negative values of ΔG° were calculated at all the studied temperatures thus proving the spontaneity of the adsorption process. The decrease of ΔG° with an increase in temperature further shows that the adsorption becomes more favourable at higher temperatures.

3.6. Adsorption kinetics

The Cr(VI) concentration in the solution as a function of contact time is shown in Fig. 8. It is observed that the Cr(VI) concentration decreases rapidly in the first 30 min followed by a slower decrease until equilibrium is reached. The rapid removal rate observed initially is due to the availability of a large number of vacant active sites that provide a surface for the adsorption of Cr(VI). The presence of vacant sites creates an adsorption gradient between the adsorbate ions and the adsorbent which leads to the adsorption. As the adsorption progresses, most of the active sites are occupied and thus a decrease in the adsorption gradient. When equilibrium is reached, all the active sites are occupied and thus no further change in the removal rate. The time required to reach equilibrium is also observed to depend on the initial concentration of Cr (VI) in the solution with more time required for higher initial concentration. Equilibrium is reached within 24 h for all the concentrations studied in this paper and no further change in concentration was observed after 24 h. This is consistent with other results from the literature [57] which demonstrated an apparent equilibrium after approximately 10 min, which was followed by a continued removal of Cr(VI) for as long as 180 min. This subsequent slower removal was attributed to a Cr(VI) reduction phase following the initial adsorption. The in situ reduction of Cr(VI) to Cr(III) after adsorption has been well-documented in the literature [58–60].

The fitting of the kinetic data on kinetic models is shown in Fig. 8(b, c, d) and the parameters obtained from the fitting are given in Table 4. The two-phase Langmuir model is observed to fit the data more accurately compared to the PFO and PSO models. The rate constant is observed to decrease with an increase in the initial concentration of Cr (VI) for both the PFO and PSO models. The calculated equilibrium uptake of Cr(VI) increases with an increase in the initial concentration of Cr (VI) for all models. The rate constants calculated from the TPA model do not follow the trend for the other two models.

Table 3
Thermodynamic parameters for adsorption of Cr(VI).

Isotherm	Temperature (K)	ΔG° (J/mol)	ΔH° (kJ/mol)	ΔS° (J/mol/K)	R^2 (linear fit)
Freundlich	298	-43215	30.3	246.8	0.991
	308	-45839			
	318	-48145			
Two-surface Langmuir	298	-27790	50.8	263.7	1.000
	308	-30388			
	318	-33066			

3.7. Effect of competing ions

In industries where chromium is used such as electroplating, paint production, and paper and dye manufacturing, a few other metals are also used and hence the discharge wastewater may contain other metals such as zinc, copper, metal sulfate, and metal nitrates [45]. Fig. 9 shows the effect of other ions (copper (Cu^{2+}), zinc (Zn^{2+}), sulfate (SO_4^{2-}) and nitrate (NO_3^-)) on the Cr(VI) removal efficiency. An insignificant increase in the percentage removal of Cr(VI) is observed in the presence of other ions even when their concentrations is increased. The percentage removal of Cr(VI) increases from 94% to 96.8% when the concentration of other ions is increased from 50 to 150 mg/L. The results suggest that the competing ions have no significant effect on the overall effectiveness of the PANI-NSA/$NiFe_2O_4$ in the removal of Cr(VI). A further study to check effect of individual ions is suggested for a better conclusion.

3.8. Reusability studies

Reusability studies were done to determine the ability of PANI-NSA/$NiFe_2O_4$ to be re-used in the removal of Cr(VI). The results are shown in Fig. 10.

The material could effectively be recovered and re-used for 5 cycles. A slight decline in Cr(VI) was observed after the second adsorption cycle of using PANI-NSA/$NiFe_2O_4$ indicating a change in the chemical composition of the material after a second cycle. The Cr(VI) removal efficiency is still above 80% for the first 3 cycles which indicates that PANI-NSA/$NiFe_2O_4$ is effective and can be reused. These results further confirm that PANI-NSA/$NiFe_2O_4$ is an excellent adsorbent for industrial applications.

3.9. Test on real chromium water

An effect of dose study with real chromium wastewater was done and the results are shown in Fig. 11. The results show that the removal efficiency of PANI-NSA/$NiFe_2O_4$ is slightly lower when using real chromium wastewater compared to when using the synthetic wastewater. This could be due to the presence of other competing ions in the real wastewater. The removal efficiency is observed to increase with an increase in dosage with a complete removal observed at 40 mg dosage. These results are consistent with effect of dosage study on synthetic water and therefore confirm that PANI-NSA/$NiFe_2O_4$ can be applied in removal of Cr(VI) from industrial wastewater.

3.10. Leaching studies

Leaching studies confirmed the presence of and Ni and Fe in the solution both after adsorption and desorption procedures at pH 2. This indicates that the synthesized PANI-NSA/$NiFe_2O_4$ is not completely stable in acidic conditions. This also explains the loss in adsorption capacity as the adsorbent was recycled since the regeneration was done using HNO_3 as part of the procedure. Further studies to check and improve the stability of PANI-NSA/$NiFe_2O_4$ at extreme pH conditions is recommended by the authors.

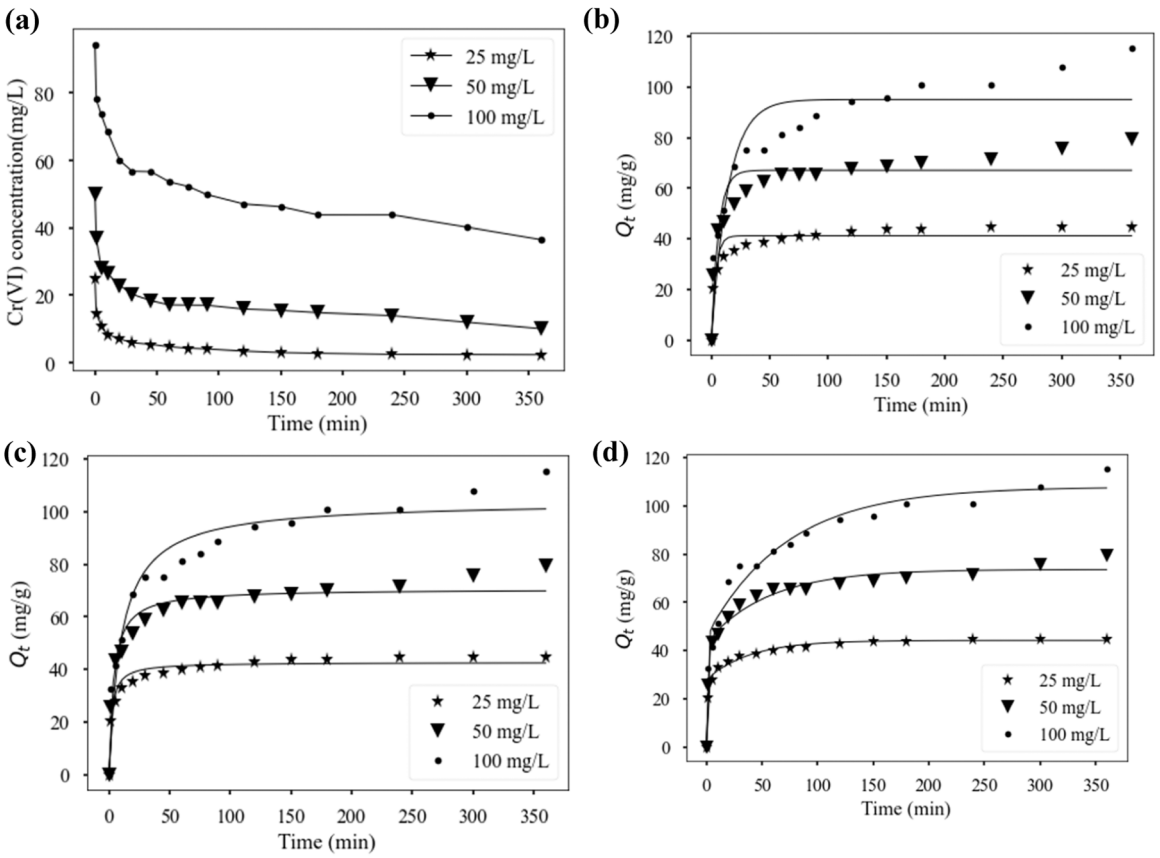

Fig. 8. The effect of time on concentration (a), (b) pseudo-first order, (c) pseudo-second-order and (d) Two-phase adsorption models fitting.

Table 4
Kinetic parameters fitted from the models.

Kinetic model	Differential form	Fitted Parameters	Concentration (mg/L)		
			25	50	100
Pseudo first order	$\frac{dQ}{dt} = k_1(Q_e - Q_t) \therefore Q_t = Q_e(1 - e^{-k_1 t})$	Q_e	41.24	67.12	95.10
		k_1	0.2761	0.1672	0.0693
		R^2	0.876	0.875	0.850
Pseudo second order	$\frac{dQ_t}{dt} = k_1(Q_e - Q_t)^2 \therefore Q_t = \frac{k_2 Q_e^2 t}{1 + k_2 Q_e t}$	k_2	0.0118	0.00384	0.00095
		Q_e	42.7	70.58	103.88
		R^2	0.9523	0.9461	0.9232
Two phase adsorption	$\begin{cases} \frac{dQ_{t,fast}}{dt} = k_{fast}(Q_{e,fast} - Q_{t,fast}), \\ \frac{dQ_{t,slow}}{dt} = k_{slow}(Q_{e,slow} - Q_{t,slow}) \quad \therefore Q_t = Q_{e,fast}(1 - e^{-k_{fast}t}) + (Q_e - Q_{e,fast})(1 - e^{-k_{slow}t}) \\ Q_{t,fast} + Q_{t,slow} = Q_t \\ Q_{e,fast} + Q_{e,slow} = Q_e \end{cases}$	k_{slow}	0.02547	0.01795	0.0139
		k_{fast}	1.272	0.8401	1.1485
		$q_{e,slow}$	16.28	30.2	62.031
		$q_{e,fast}$	27.97	43.41	45.79
		R^2	0.9941	0.985	0.9774

3.11. Comparison with other adsorbents

A comparison of maximum adsorption capacity between PANI-NSA/$NiFe_2O_4$ and other adsorbents was done and is given in Table 5. The comparison shows that PANI-NSA/$NiFe_2O_4$ is a better-performing adsorbent for the removal of Cr(VI).

3.12. Proposed mechanism of adsorption

Fig. 12 (a) shows the comparison between the total Cr and Cr(VI) available in the solution after adsorption. The comparison between total Cr and Cr(VI) concentration with time (Fig. 12 (b)) shows that initially total Cr is equal to Cr(VI) thus no Cr(III) present. As time goes, the total Cr is more than Cr(VI) thus presence of Cr(III). The presence of Cr(III) in the solution proves that some of the Cr(VI) get adsorbed by PANI-NSA/$NiFe_2O_4$ is reduced to Cr(III) which is released back to the solution. The deconvoluted chromium peaks from the XPS (Fig. 12 (c)) show the presence of both Cr(VI) and Cr(III) on the surface of PANI-NSA/$NiFe_2O_4$ which further confirms the reduction of Cr(VI) to Cr(III).

Therefore, from the XPS results and the comparison between total Cr and Cr(VI) present in the solution, the mechanism of Cr(VI) removal by PANI-NSA/$NiFe_2O_4$ involves adsorption of Cr(VI) onto the surface of PANI-NSA/$NiFe_2O_4$ and then reduction of Cr(VI) to Cr(III). Some of the Cr(III) is adsorbed onto the PANI-NSA/$NiFe_2O_4$ surface while part of the Cr(III) is released back into the solution. Consequently, Cr(VI) removal is believed to occur in two stages:

1. In acidic conditions (in the pH range 2–6), dichromate oxyanion is hydrolysed to $HCrO_4^-$ which electrostatically interacts with the

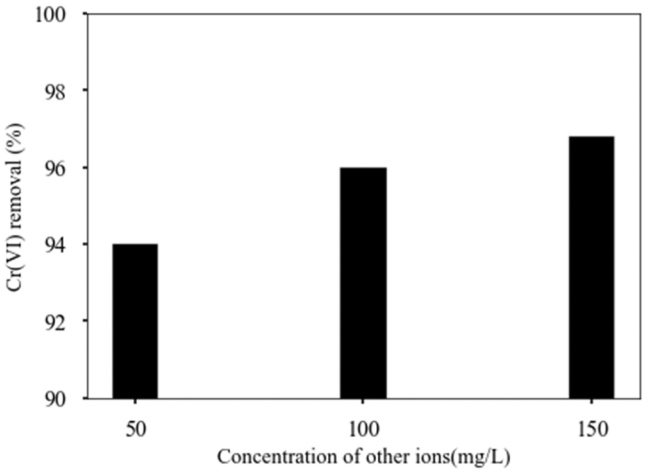

Fig. 9. Effect of other ions on the removal of Cr(VI).

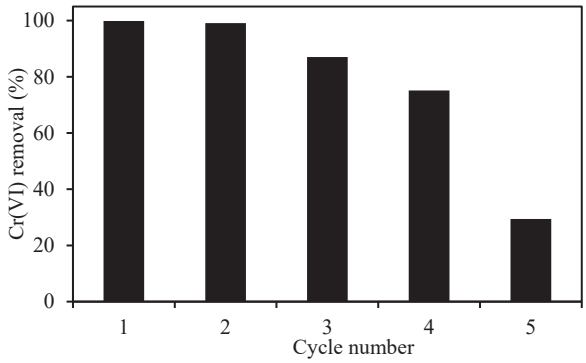

Fig. 10. Recycling of PANI-NSA/$NiFe_2O_4$ for the removal of Cr(VI).

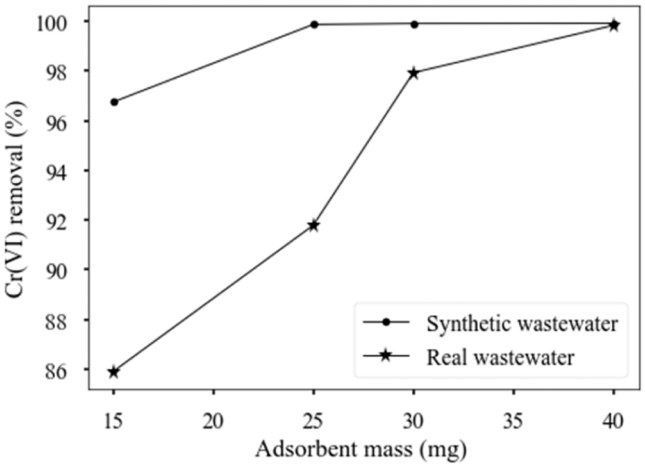

Fig. 11. Effect of dose study on real chromium wastewater as compared to synthetic wastewater.

positively charged amine groups from PANI-NSA/$NiFe_2O_4$ while at higher pH values (above 6), dichromate oxyanion are the most valent and are removed by binding with the protonated amine group from PANI −NSA/$NiFe_2O_4$ leading to Cr(VI) removal via adsorption:

$$CrO_7^{2-} + H_2O \leftrightarrow 2HCrO_4^-$$

$$-NH_3^+ + HCrO_4^- \quad = \quad -NH_3^+ - - - HCrO_4^-$$

Table 5
Comparison of PANI-NSA/$NiFe_2O_4$ and other PANI based adsorbents studied for Cr(VI) removal.

Name of the material	Q_m (mg/g)	Temperature (°C)	pH	Reference
Polypyrrole/Fe_3O_4 nanocomposite	169.49	25	2.0	[61]
Polypyrrole/maghemite	209	Room temperature	2.0	[62]
Polyaniline/maghemite	196	Room temperature	2.0	[62]
Polyaniline-coated date seed biochar	27.3	50	5.0	[63]
Polyaniline@ magnetic chitosan	186.6	25	2.0	[64]
Polyaniline/ZnO	120.92	30	2.0	[65]
Polyaniline	198.67	15	3.0	[66]
Polyaniline coated PVDF-HFP	15.08	24	4.5	[67]
Tea waste/Fe_3O_4	75.76	45	2	[4]
PANI-NSA/$NiFe_2O_4$	420.0	45	2.0	This study

$$-NH_3^+ + CrO_7^{2-} \quad = \quad -NH_3^+ - - - CrO_7^{2-}$$

2. Cr(VI) is subsequently reduced to Cr(III) due to the presence of electron donors of PANI:

$$HCrO_4^- + 7H^+ + 3e^- \leftrightarrow Cr^{3+} + 4H_2O$$

The overall mechanism is represented by the schema in Fig. 13.

4. Conclusion

The removal of Cr(VI) from aqueous solution using PANI-NSA/$NiFe_2O_4$ nanocomposite was studied. The maximum removal efficiency (99%) of Cr(VI) was observed at a pH value of 2 and adsorbent loading of 0.5 g/L. Surface functional groups determined by XPS proved that Cr (VI) is reduced to Cr(III) which attaches on the surface of PANI-NSA/$NiFe_2O_4$ with some released back into the solution. A maximum adsorption capacity of 420 mg/g at 45 °C was calculated using the Langmuir isotherm model. Compared to other materials from the literature, the adsorption capacity of PANI-NSA/$NiFe_2O_4$ was higher. The two-phase Langmuir kinetic model best fitted the kinetic data from the experiment. The effect of other ions on the removal of Cr(VI) was minimal proving that the material is effective even in the presence of other ions and hence can effectively be applied in industrial wastewater treatment. Up to 87% Cr(VI) removal efficiency could be achieved for three adsorption cycles hence PANI-NSA/$NiFe_2O_4$ can effectively be recycled. When using real chromium wastewater, it was observed that 40 mg of PANI-NSA/$NiFe_2O_4$ could achieve 100% Cr(VI) removal efficiency from 50 mL solution with 50 mg/L initial concentration.

CRediT authorship contribution statement

Ruth Kasavo: Conceptualization, Investigation, Methodology, Data curation, Validation, Visualisation, Writing - original draft, Formal analysis, Writing - review & editing. **Madhumita Bhaumik**: Conceptualization, Methodology, Writing - original draft, Writing - review & editing, Formal analysis, Supervision. **HG Brink**: Data curation, Software, Formal analysis, Writing - original draft, Writing - review & editing, Funding acquisition, Resources, Supervision.

Declaration of Competing Interest

The authors declare that they have no known competing financial interests or personal relationships that could have appeared to influence

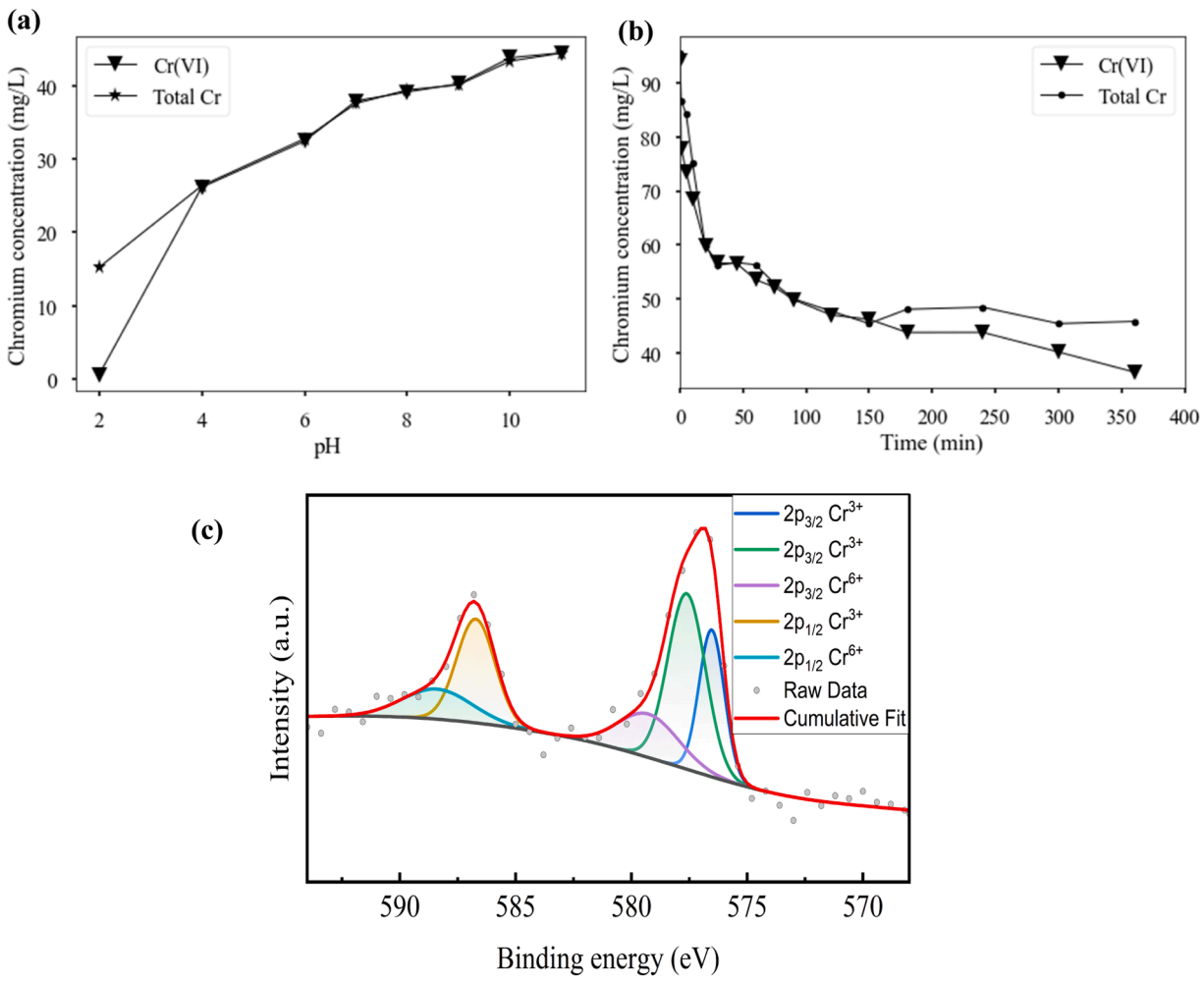

Fig. 12. Concentration of Cr(VI) and total Cr under different parameters (a) pH, (b) contact time and (c) XPS speciation analysis of Cr.

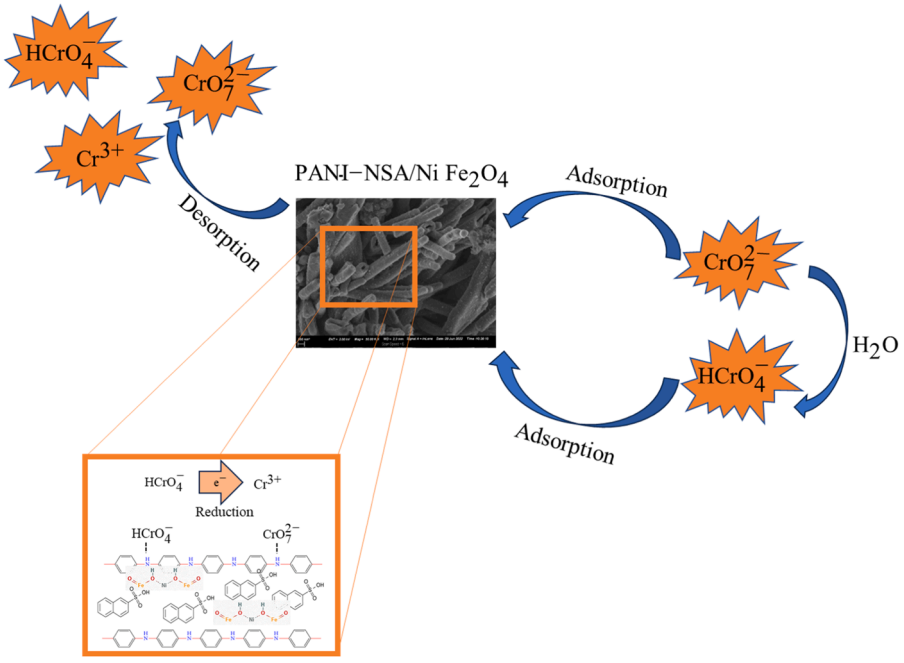

Fig. 13. Schematic representation of the proposed adsorption-reduction mechanism responsible for Cr(VI) removal by PANI-NSA/ $NiFe_2O_4$.

the work reported in this paper.

Data availability

Data will be made available on request.

Acknowledgements

The authors would like to thank the National Research Funding (NRF) of South Africa who funded the research through Research Grants UID-132732 and CSRP220420402.

References

[1] A. Samadi, et al., Polyaniline-based adsorbents for aqueous pollutants removal: a review, Chem. Eng. J. 418 (2021), 129425.
[2] M.S. Samuel, et al., Clean approach for chromium removal in aqueous environments and role of nanomaterials in bioremediation: present research and future perspective, Chemosphere 284 (2021), 131368.
[3] J. Briffa, E. Sinagra, R. Blundell, Heavy metal pollution in the environment and their toxicological effects on humans, Heliyon 6 (9) (2020), e04691.
[4] S. Fan, et al., Facile synthesis of tea waste/Fe 3 O 4 nanoparticle composite for hexavalent chromium removal from aqueous solution, RSC Adv. 7 (13) (2017) 7576–7590.
[5] H. Karimi-Maleh, et al., Recent advances in removal techniques of Cr (VI) toxic ion from aqueous solution: a comprehensive review, J. Mol. Liq. 329 (2021), 115062.
[6] S. Xia, et al., A critical review on bioremediation technologies for Cr (VI)-contaminated soils and wastewater, Crit. Rev. Environ. Sci. Technol. 49 (12) (2019) 1027–1078.
[7] H. Liu, X. Yu, Hexavalent chromium in drinking water: Chemistry, challenges and future outlook on Sn (II)-and photocatalyst-based treatment, Front. Environ. Sci. Eng. 14 (5) (2020) 1–9.
[8] R. Rakhunde, L. Deshpande, H. Juneja, Chemical speciation of chromium in water: a review, Crit. Rev. Environ. Sci. Technol. 42 (7) (2012) 776–810.
[9] M. Agarwal, K. Singh, Heavy metal removal from wastewater using various adsorbents: a review, J. Water Reuse Desalin. 7 (4) (2017) 387–419.
[10] D.R. Rout, H.M. Jena, Synthesis of novel epichlorohydrin cross-linked β-cyclodextrin functionalized with reduced graphene oxide composite adsorbent for treatment of phenolic wastewater, Environ. Sci. Pollut. Res. 29 (48) (2022) 73444–73460.
[11] N. Sharma, et al., Heavy metal pollution: insights into chromium eco-toxicity and recent advancement in its remediation, Environ. Nanotechnol., Monit. Manag. 15 (2021), 100388.
[12] A. Anjum, et al., A review of novel green adsorbents as a sustainable alternative for the remediation of chromium (VI) from water environments, Heliyon 9 (5) (2023), e15575.
[13] K. Jahan, N. Kumar, V. Verma, Removal of hexavalent chromium from potable drinking using a polyaniline-coated bacterial cellulose mat, Environ. Sci.: Water Res. Technol. 4 (10) (2018) 1589–1603.
[14] K. Shekhawat, S. Chatterjee, B. Joshi, Chromium toxicity and its health hazards, Int. J. Adv. Res 3 (7) (2015) 167–172.
[15] X. Xing, et al., A comprehensive review on emerging natural and tailored materials for chromium-contaminated water treatment and environmental remediation, J. Environ. Chem. Eng. 10 (2) (2022), 107325.
[16] H. Arslan, et al., Comparison of Cr (VI) adsorption and photocatalytic reduction efficiency using leonardite powder, Chemosphere 300 (2022), 134492.
[17] B. Panneerselvam, S. Priya K, Phytoremediation potential of water hyacinth in heavy metal removal in chromium and lead contaminated water. Int. J. Environ. Anal. Chem. 103 (13) (2023) 3081–3096.
[18] A. Gautam, A. Kushwaha, R. Rani, Microbial remediation of hexavalent chromium: An eco-friendly strategy for the remediation of chromium-contaminated wastewater. The Future of Effluent Treatment Plants, Elsevier, 2021, pp. 361–384.
[19] S.-Y. Pi, et al., Cr (VI) reduction coupled with Cr (III) adsorption/precipitation for Cr (VI) removal at near neutral pHs by polyaniline nanowires-coated polypropylene filters, J. Taiwan Inst. Chem. Eng. 123 (2021) 166–174.
[20] J. Lu, et al., Simultaneous removal of Cr (VI) and Cu (II) from acid wastewater by electrocoagulation using sacrificial metal anodes, J. Mol. Liq. 359 (2022), 119276.
[21] J. Geng, et al., Adsorption of Cr (VI) and dyes by plant leaves: effect of extraction by ethanol, relationship with element contents and adsorption mechanism, Ind. Crops Prod. 177 (2022), 114522.
[22] H. Khurshid, M.R.U. Mustafa, M.H. Isa, Adsorption of chromium, copper, lead and mercury ions from aqueous solution using bio and nano adsorbents: a review of recent trends in the application of AC, BC, nZVI and MXene, Environ. Res. 212 (2022), 113138.
[23] N.H. Kera, et al., Selective removal of toxic Cr (VI) from aqueous solution by adsorption combined with reduction at a magnetic nanocomposite surface, J. Colloid Interface Sci. 503 (2017) 214–228.
[24] X. Liu, et al., Magnetic red mud/chitosan based bionanocomposites for adsorption of Cr (VI) from aqueous solutions: synthesis, characterization and adsorption kinetics, Polym. Bull. 80 (2) (2023) 2099–2118.
[25] A. Abushawish, et al., High-efficiency removal of hexavalent chromium from contaminated water using nitrogen-doped activated carbon: Kinetics and isotherm study, Mater. Chem. Phys. 291 (2022), 126758.
[26] J. Feng, et al., Atomic layer deposition of TiO2 on carbon-nanotubes membrane for capacitive deionization removal of chromium from water, Chin. J. Chem. Eng. 45 (2022) 15–21.
[27] H. Yuan, et al., Metal-organic frameworks encapsulated Ag nanoparticle-nanoclusters with enhanced luminescence for simultaneous detection and removal of chromium (VI), Microchem. J. 181 (2022), 107722.
[28] M.A. Lala, et al., Adsorption of hexavalent chromium from aqueous solution using cationic modified rice husk: Parametric optimization via Taguchi design approach, Sci. Afr. 20 (2023), e01633.
[29] S. Hu, et al., Efficient reduction and adsorption of Cr(VI) using FeCl3-modified biochar: synergistic roles of persistent free radicals and Fe(II), J. Environ. Sci. 137 (2024) 626–638.
[30] Y. Fei, Y.H. Hu, Design, synthesis, and performance of adsorbents for heavy metal removal from wastewater: a review, J. Mater. Chem. A 10 (3) (2022) 1047–1085.
[31] Y. Jiang, et al., Polyaniline-based adsorbents for removal of hexavalent chromium from aqueous solution: a mini review, Environ. Sci. Pollut. Res. 25 (7) (2018) 6158–6174.
[32] P. Singh, S. Shukla, Advances in polyaniline-based nanocomposites, J. Mater. Sci. 55 (4) (2020) 1331–1365.
[33] L. Lohrentz, M. Bhaumik, H.G. Brink, High-capacity adsorption of hexavalent chromium by a polyaniline-Ni(0) nanocomposite adsorbent: Expanding the Langmuir-Hinshelwood kinetic model, J. Mol. Liq. 389 (2023), 122931.
[34] M. Janmohammadi, et al., Waste plastic filter modified with polyaniline and polypyrrole nanoparticles for hexavalent chromium removal, Sci. Total Environ. 752 (2021), 141850.
[35] F.-L. Long, et al., Highly efficient removal of hexavalent chromium from aqueous solution by calcined Mg/Al-layered double hydroxides/polyaniline composites, Chem. Eng. J. 404 (2021), 127084.
[36] R. Das, et al., Silver decorated magnetic nanocomposite (Fe3O4@ PPy-MAA/Ag) as highly active catalyst towards reduction of 4-nitrophenol and toxic organic dyes, Appl. Catal. B: Environ. 244 (2019) 546–558.
[37] N. Gupta, et al., Current development in synthesis and characterization of nickel ferrite nanoparticle, Mater. Today.: Proc. 4 (2) (2017) 342–349.
[38] T. Shanmugavel, et al., Tailoring the structural and magnetic properties and of nickel ferrite by auto combustion method, Procedia Mater. Sci. 6 (2014) 1725–1730.
[39] L.P. Lingamdinne, et al., Studies on removal of Pb (II) and Cr (III) using graphene oxide based inverse spinel nickel ferrite nano-composite as sorbent, Hydrometallurgy 165 (2016) 64–72.
[40] S. Agrawal, N. Singh, Removal of toxic hexavalent chromium from aqueous solution by nickel ferrite-polyaniline nanocomposite, Desalin. Water Treat. 57 (38) (2016) 17757–17766.
[41] Y. Long, et al., Electrical and magnetic properties of polyaniline/Fe3O4 nanostructures, Phys. B: Condens. Matter 370 (1–4) (2005) 121–130.
[42] U.O. Aigbe, et al., A novel method for removal of Cr (VI) using polypyrrole magnetic nanocomposite in the presence of unsteady magnetic fields, Sep. Purif. Technol. 194 (2018) 377–387.
[43] M.S. Samuel, et al., Preparation of graphene oxide/chitosan/ferrite nanocomposite for Chromium (VI) removal from aqueous solution, Int. J. Biol. Macromol. 119 (2018) 540–547.
[44] G. Castellar-Ortega, et al., Equilibrium, kinetic and thermodynamic of direct blue 86 dye adsorption on activated carbon obtained from manioc husk, Rev. MVZ Córdoba 24 (2) (2019) 7231–7238.
[45] M. Bhaumik, V.K. Gupta, A. Maity, Synergetic enhancement of Cr (VI) removal from aqueous solutions using polyaniline@ Ni (OH) 2 nanocomposites adsorbent, J. Environ. Chem. Eng. 6 (2) (2018) 2514–2527.
[46] M. Bhaumik, et al., Tunability of localization length in naphthalene sulfonic acid doped polyaniline/nickel ferrite composite nanorods system, J. Appl. Phys. 126 (3) (2019), 035102.
[47] C. Basavaraja, et al., Electrical properties of colloidal polyaniline-2-naphthalene sulfonic acid/graphene nanoparticle composite films, Polym. Compos. 35 (1) (2014) 60–67.
[48] C. Terraza, et al., Preparation of CuONPs@PVDF/non-woven polyester composite membrane: structural influence of nanoparticle addition, Polymers 10 (2018) 862.
[49] D.C. Lingegowda, et al., FTIR spectroscopic studies on Cleome gynandra–comparative analysis of functional group before and after extraction, Rom. J. Biophys. 22 (3–4) (2012) 137–143.
[50] N. Macherla, et al., Improved performance of flexible supercapacitor using naphthalene sulfonic acid-doped polyaniline/sulfur-doped reduced graphene oxide nanocomposites, Int. J. Energy Res. 46 (5) (2022) 6529–6542.
[51] G. Yang, et al., Effective removal of Cr (VI) through adsorption and reduction by magnetic mesoporous carbon incorporated with polyaniline, RSC Adv. 4 (102) (2014) 58362–58371.
[52] H.M. Hamadeen, E.A. Elkhatib, M.L. Moharem, Optimization and mechanisms of rapid adsorptive removal of chromium (VI) from wastewater using industrial waste derived nanoparticles, Sci. Rep. 12 (1) (2022) 14174.
[53] M. Asanu, D. Beyene, A. Befekadu, Removal of hexavalent chromium from aqueous solutions using natural zeolite coated with magnetic nanoparticles: optimization, kinetics, and equilibrium studies, Adsorpt. Sci. Technol. (2022) **2022**.
[54] R. Karthik, S. Meenakshi, Removal of hexavalent chromium ions using polyaniline/silica gel composite, J. Water Process Eng. 1 (2014) 37–45.

[55] H.N. Tran, S.J. You, H.P. Chou, Thermodynamic parameters of cadmium adsorption onto orange peel calculated from various methods: a comparison study, J. Environ. Chem. Eng. 4 (3) (2016) 2671–2682.
[56] Guo, L., C. Verma, and D. Zhang, *17.4.1 Physisorption, in Eco-Friendly Corrosion Inhibitors - Principles, Designing and Applications*. Elsevier. p. 300.
[57] K.L. Muedi, et al., Rapid removal of Cr (VI) from aqueous solution using polycationic/di-metallic adsorbent synthesized using Fe3+/Al3+ recovered from real acid mine drainage, Minerals 12 (10) (2022) 1318.
[58] Y. Chen, et al., Reduction and removal of chromium VI in water by powdered activated carbon, Materials 11 (2) (2018) 269.
[59] F. Liu, et al., Adsorption and reduction of Cr (VI) from aqueous solution using cost-effective caffeic acid functionalized corn starch, Chemosphere 279 (2021), 130539.
[60] X. Liu, et al., Adsorption-reduction of Cr (VI) with magnetic Fe-CN composites, Water 15 (12) (2023) 2290.
[61] M. Bhaumik, et al., Chromium (VI) removal from water using fixed bed column of polypyrrole/Fe3O4 nanocomposite, Sep. Purif. Technol. 110 (2013) 11–19.
[62] A.E. Chávez-Guajardo, et al., Efficient removal of Cr (VI) and Cu (II) ions from aqueous media by use of polypyrrole/maghemite and polyaniline/maghemite magnetic nanocomposites, Chem. Eng. J. 281 (2015) 826–836.
[63] S. Tripathy, et al., Efficient removal of Cr (VI) by polyaniline modified biochar from date (Phoenix dactylifera) seed, Groundwater Sustain. Dev. 15 (2021), 100653.
[64] C. Lei, et al., Polyaniline@ magnetic chitosan nanomaterials for highly efficient simultaneous adsorption and in-situ chemical reduction of hexavalent chromium: Removal efficacy and mechanisms, Sci. Total Environ. 733 (2020), 139316.
[65] R. Ahmad, Polyaniline/ZnO nanocomposite: a novel adsorbent for the removal of Cr (VI) from aqueous solution, Adv. Compos. Mater. Dev. (2019) 1–22.
[66] K. Zhu, et al., Polyaniline-modified Mg/Al layered double hydroxide composites and their application in efficient removal of Cr (VI), ACS Sustain. Chem. Eng. 4 (8) (2016) 4361–4369.
[67] G. Dognani, et al., Effective chromium removal from water by polyaniline-coated electrospun adsorbent membrane, Chem. Eng. J. 372 (2019) 341–351.